Supporting Information

Self-Supported PPy-Encapsulated CoS_2 Nanosheets Anchored on TiO_{2-x} Nanorod Arrays Support by Ti–S Bonds for Ultra-long Life Hybrid Mg^{2+}/Li^{+} Battery

Chao Liu,[b] Guangyu Zhao,[a] Li Zhang,[b] Pengbo Lyu,*[c] Xianbo Yu,[b] Huihuang Huang,[b] Guillaume Maurin,[c] Kening Sun[a] and Naiqing Zhang*[a]*

[a] Interdisciplinary Science Research Center, Harbin Institute of Technology, Harbin, Heilongjiang, 150001, China

[b] School of Chemistry and Chemical Engineering, Harbin Institute of Technology, Harbin, Heilongjiang, 150001, China

[c] Institut Charles Gerhardt Montpellier, UMR 5253 CNRS, Université de Montpellier, Montpellier, 34095, France

* E-mail: zhaogy810525@gmail.com; pengbo.lyu@umontpellier.fr; znqmww@163.com.

Experimental Section

Characterizations

Materials Characterization: The scanning electron microscope (SEM) images and energy dispersive X-ray spectroscopy (EDS) were obtained in Hitachi Su-8010. The X-ray diffraction (XRD) patterns were performed on a PANalytical X'pert PRO X-ray diffractometer with Cu Ka radiation (λ=1.5418 Å). X-ray photoelectron spectra (XPS) were performed with a K-Alpha electron spectrometer (Thermofish Scientific Company) using Al Ka (1486.6 eV) radiation. The binding energies were referenced to the C 1s line at 284.8 eV from adventitious carbon. Transmission electron microscope (TEM) images were performed on a JEOL-2100. The thermogravimetric analysis (TGA) was performed on a Shimadzu DRG-60.

Electrochemical experiments: The TiO_{2-x}@CoS_2@PPy and TiO_2@CoS_2@PPy were used as the electrode without additional conductive additive and insulating binder. The battery tests of TiO_{2-x}@CoS_2@PPy and TiO_2@CoS_2@PPy in MLIB and MRB were carried out with the CR2035 button testing batteries using Celgard 2400 as the microporous membrane and Mg foil as the counter electrode. A 0.4 M APC/THF electrolyte was used as the MRB electrolyte. The MLIB electrolyte was prepared by adding 0.4 M LiCl into the 0.4 M APC/THF. A BTS-2000 Neware Battery Testing System was employed for discharge/charge testing with voltage range from 0.01 to 1.80 V *vs.* Mg^{2+}/Mg. The cyclic voltammetry (CV) of the batteries was carried out on the CHI 660 electrochemical workstation with voltage range from 0.01 to 1.80 V *vs.* Mg^{2+}/Mg at a scan rate of 0.1 mV s^{-1} under ambient temperature. The electrochemical impedance spectra (EIS) tests were investigated by PARSTAT 2273 advanced electrochemical system, and the frequency range from 1 MHz to 1Hz, the measurement time is about 24 h after cell assembly. The stability potential window of TiO_{2-x} substrate in APC-LiCl electrolytes was investigated by liner sweep voltammetry (LSV) measurements from open circuit potential to 3.0 V *vs.* Mg^{2+}/Mg. at a scan rate of 1 mV s^{-1}.

The Li^+ diffusion coefficient is tested by using Galvanostatic Intermittent Titration Technique (GITT) from the potential response to a small constant current pulse (100 mA g^{-1}), and calculated based on as follows:[1]

$$D = \frac{4}{\pi\tau}\left(\frac{m_B V_M}{M_B S}\right)^2\left(\frac{\Delta E_S}{\Delta E_t}\right)^2$$

τ: the relaxation time (here is 3600 s);

m_B, V_M, S, and M_B are the mass, molar volume, electrode-electrolyte interface area, and molar mass of TiO_{2-x}@CoS_2@PPy or TiO_2@CoS_2@PPy, respectively.

ΔE_s: the steady-state potential change (V) by the current pulse;

ΔE_t: the potential change (V) during the constant current pulse after eliminating the iR drop;

Density functional theory (DFT) calculations

Computational details: The spin-polarized DFT calculations were performed using the projector augmented wave (PAW)[2] formalism within the generalized gradient approximation (GGA) method with Perdew-Burke-Ernzerhof (PBE) exchange-correlation functional as implemented in Vienna Ab Initio Simulation Package (VASP).[3-5] The cutoff energy of 500eV for the plane-wave basis set has been consistently used in all calculations. The convergence criterion of 0.05 eV/Å was used for the forces in geometry optimizations and 10^{-4} eV was used for the energy convergence. The DFT-D3(BJ) method of Grimme was employed to evaluate the dispersion contribution for the adsorption.[6]

Model: To model the 001 surface of anatase TiO_2, a slab contains 3 atomic layers was adopted and the bottom layer was fixed during all calculations. The lattice parameters of the surface were 3.78 Å (11.33 Å for 3×3×1 supercell). A vacuum of at least 15Å have been applied to avoid artificial interlayer interactions. In addition to the pristine 001 surface, one oxygen atom was removed to model the 001 surface with oxygen vacancy. A 2×2×1 Monkhorst-Pack grid was consistently used for the super cell models.

Calculation of Average Energy Density:

This battery capacity was calculated via following formula

$$C_{battery} = C_{anode} \times C_{cathode} / (C_{anode} + C_{cathode})$$

The average energy density was calculated via following formula

$$E_{battery} = C_{battery} \times V$$

Where V is the average discharge voltage.

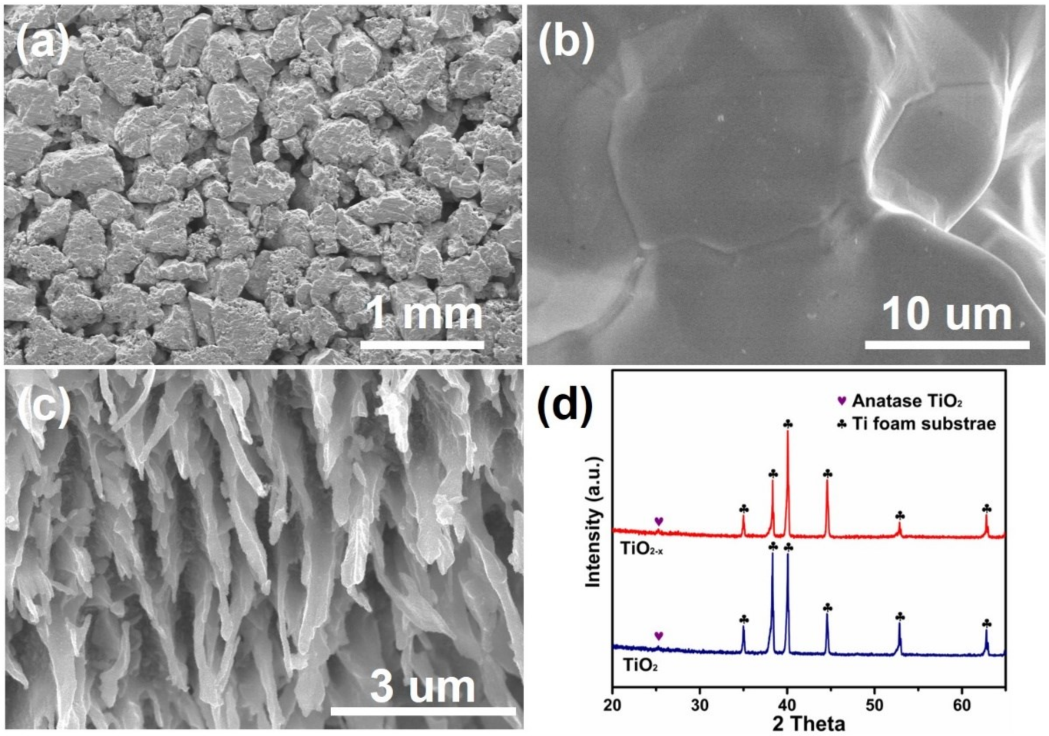

Fig. S1 SEM images of (a-b) Ti foam and (c) TiO_{2-x} nanorod arrays. (d) XRD patterns of TiO_2 nanorod arrays and TiO_{2-x} nanorod arrays.

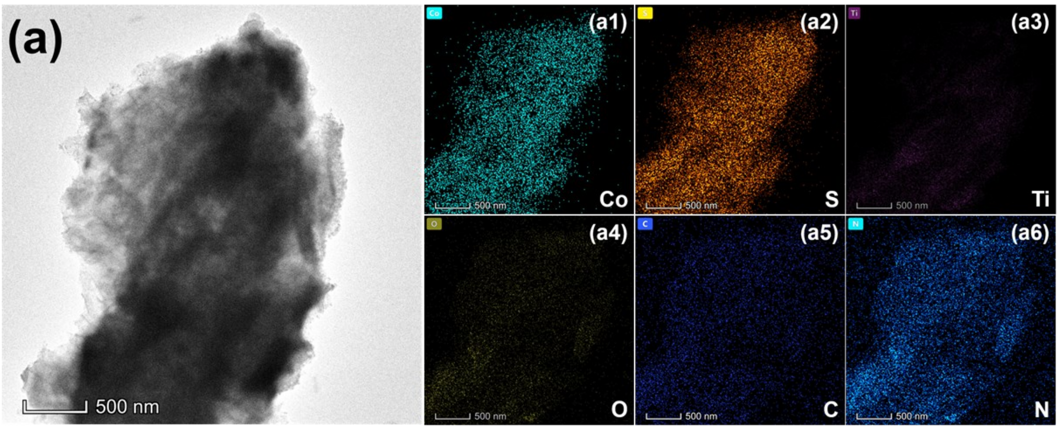

Fig. S2 (a) TEM image and (a1–6) TEM elemental mappings of TiO_{2-x}@CoS_2@PPy.

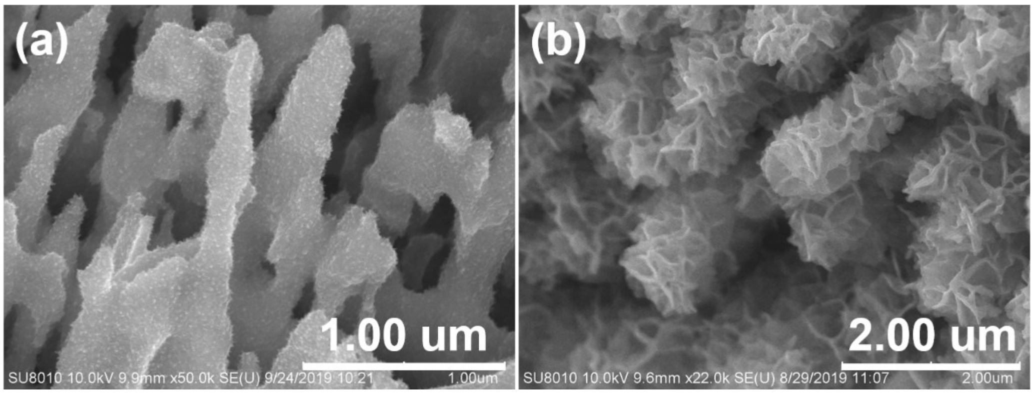

Fig. S3 SEM images of (a) TiO_2 nanorod arrays and (b) TiO_2@CoS_2@PPy.

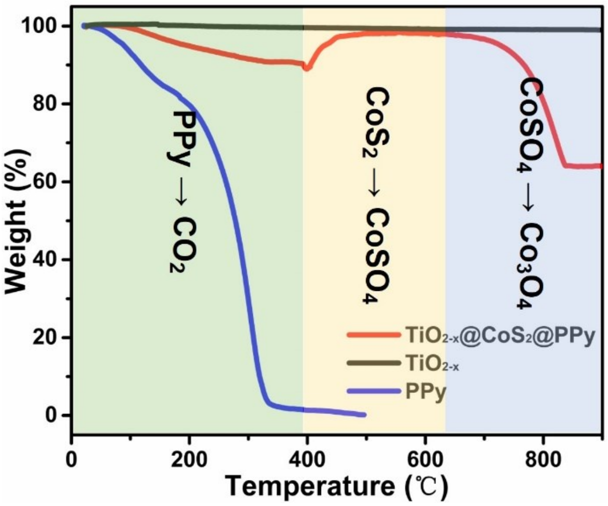

Fig. S4 TGA curves of the PPy, TiO_{2-x} and TiO_{2-x}@CoS_2@PPy in air atmosphere.

Thermogravimetric analyses of PPy, TiO_{2-x} and TiO_{2-x}@CoS_2@PPy are performed by collecting their powder. When the temperature reaches 400^{o}C, the mass of PPy has been completely lost (total of 98.7%). And the mass of TiO_{2-x} has remained essentially unchanged up to 900^{o}C. For TiO_{2-x}@CoS_2@PPy, the total weight loss is 36.1 wt.% which is ascribed to the oxidation of CoS_2 as well as the weight loss of PPy. There are three weight reactions in the TGA process, where the weight loss located at 25-350^{o}C can be attributed to the weight loss of PPy, the other weight loss located at 390-510^{o}C is ascribed to the oxidation of CoS_2 to $CoSO_4$, another weight loss located at 650-850^{o}C is assigned to the decomposition of $CoSO_4$ into Co_3O_4 and SO_2.[6,7] Thus, we can calculate the contents of CoS_2, $TiO_{2–x}$, and PPy in the $TiO_{2–x}$@CoS_2@PPy nanorods are 77.5 wt.%, 13.3 wt.%, and 9.2 wt.%, respectively.

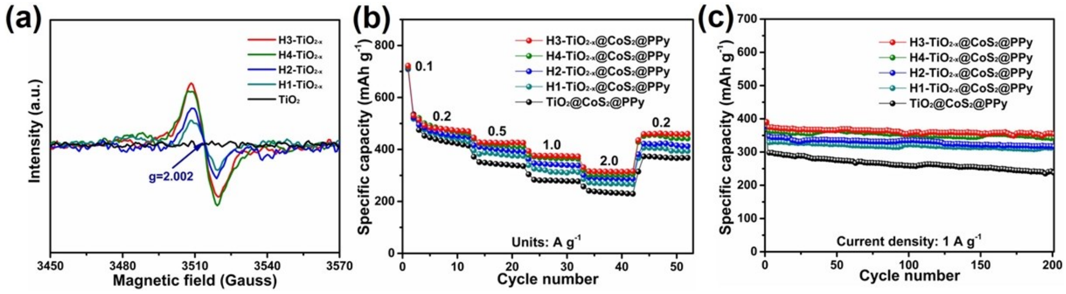

Fig. S5 (a) EPR spectra of the TiO_{2-x} nanorods with different OVs content and TiO_2 nanorods. (b) Rate capability and (c) cycling performances of the TiO_{2-x}@CoS_2@PPy with different OV contents.

In order to deeply understand the defect effect in the electrochemical performances of TiO_{2-x}@CoS_2@PPy, the $TiO_{2–x}$ nanorods with different oxygen vacancy (OV) contents were prepared by annealing titanium oxide nanorods at 600 ^{o}C in Ar/H_2 (10% H_2, 90% Ar) for different periods (1 h, 2h, 3h, and 4h). The samples obtained are named as H1-$TiO_{2–x}$, H2-$TiO_{2–x}$, H3-$TiO_{2–x}$, and H4-$TiO_{2–x}$. TiO_2 nanorods without OV were prepared by heat-treatment at 600 ^{o}C in Ar for 3 hours.

To confirm the existence and contents of OVs in H1-$TiO_{2–x}$, H2-$TiO_{2–x}$, H3-$TiO_{2–x}$, H4-$TiO_{2–x}$, and TiO_2, electro-paramagnetic resonance spectroscopy (EPR) was conducted on these control samples at room temperature, as shown in **Fig. S5a**. The H4-$TiO_{2–x}$, H3-$TiO_{2–x}$, H2-$TiO_{2–x}$, and H1-$TiO_{2–x}$ exhibit distinct EPR signal with a *g* value of 2.002, which indicates the presence of superoxide radicals ($O_2^{\bullet-}$) attached to the OVs on the surface of metal oxide materials. The intensity of EPR signals is gradually increased with prolonged annealing time, implying the increase of OV content. After annealed for more than 3 h, the H4–TiO_{2-x} and H3–TiO_{2-x} have near signal intensities, manifesting the surface of the TiO_2 nanorods has been completely converted into TiO_{2-x}. As the annealing time increasing, it is difficult for the TiO_{2-x} nanorods to form more OVs.

The rate capability and cycling performance of the TiO_{2-x}@CoS_2@PPy with different OVs content were studied. As shown in **Fig. S5b-c**, the H3-TiO_{2-x}@CoS_2@PPy and H4-TiO_{2-x}@CoS_2@PPy show the best rate capability and cycling performance, indicating the electrochemical performances becomes better as the OVs content increasing. This is because more OVs content can form strong Ti-S bonds, which are beneficial to electrode stability and electron conduction, thereby improving the electro-chemical performances of the electrodes.

H3-TiO_{2-x}@CoS_2@PPy and H4-TiO_{2-x}@CoS_2@PPy exhibit simliar OVs content and electrochemical performances. For the high efficiency of experimental preparation, we choose 3 hours as the annealing time.

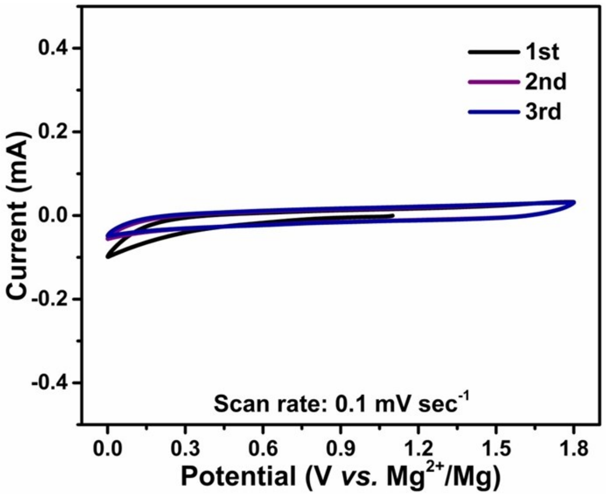

Fig. S6 CV curves of TiO_{2-x}@CoS_2@PPy in MRB at a scan of 0.1 mV s^{-1} for the first three cycles.

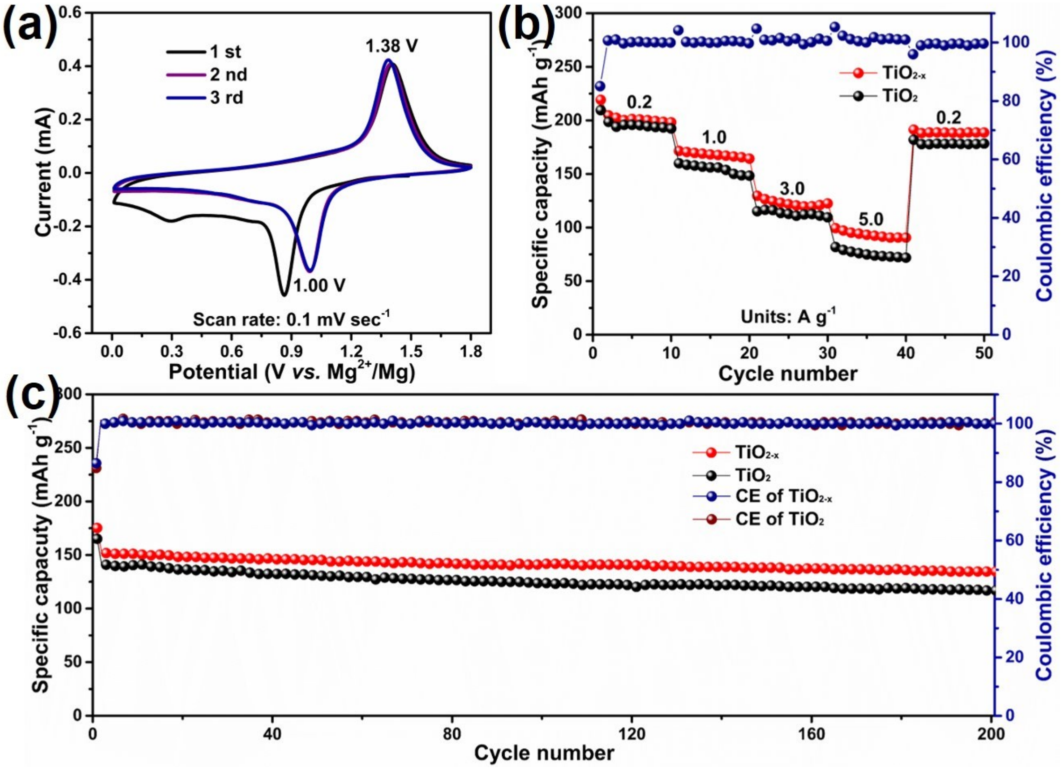

Fig. S7 (a) CV curves of TiO_{2-x} in MLIB at a scan of 0.1 mV s^{-1} for the first three cycles. (b) Rate performance of TiO_{2-x} and TiO_2 in MLIB. (c) Cycle stability of TiO_{2-x} and TiO_2 in MLIB at 1.0 A g^{-1}.

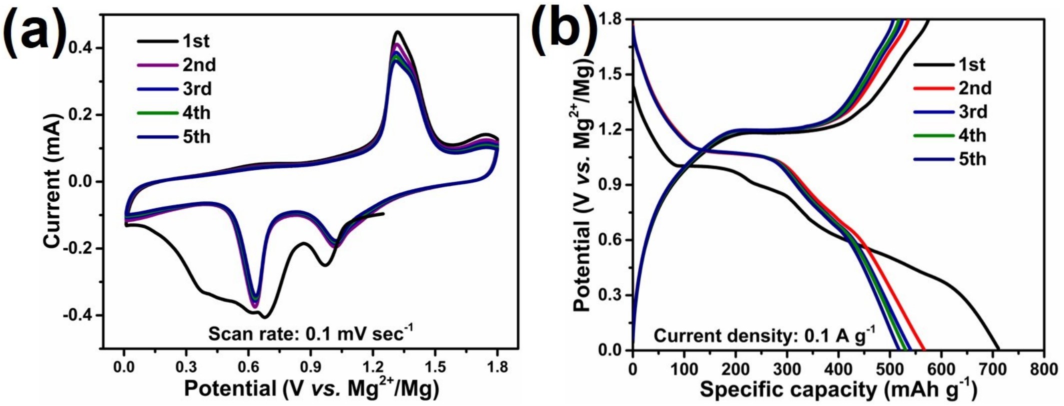

Fig. S8 (a) CV curves of $TiO_2@CoS_2@PPy$ in MLIB at a scan of 0.1 mV s^{-1} for the first five cycles. (b) Discharge/charge curves of $TiO_2@CoS_2@PPy$ for the first five cycles at 0.1 A g^{-1}.

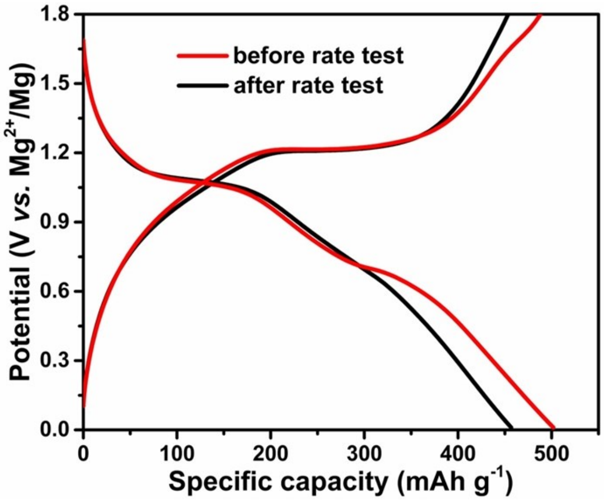

Fig. S9 Comparison of the 2nd and after-rate-test discharge/charge curves of TiO_{2-x}@CoS_2@PPy electrode at 0.2 A g^{-1}.

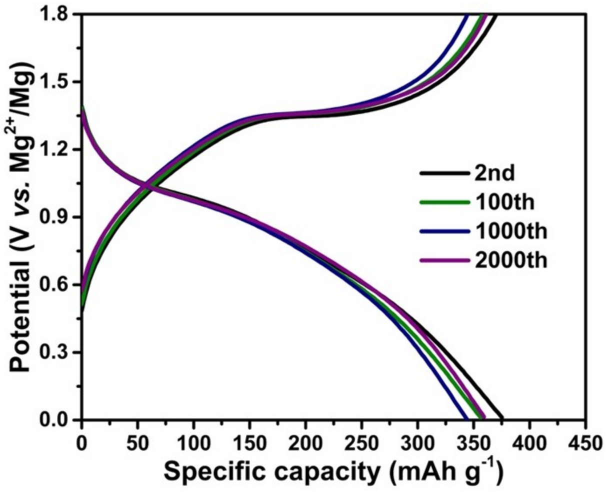

Fig. S10 Charge/discharge curves of TiO_{2-x}@CoS_2@PPy for different cycles at 1 A g^{-1}.

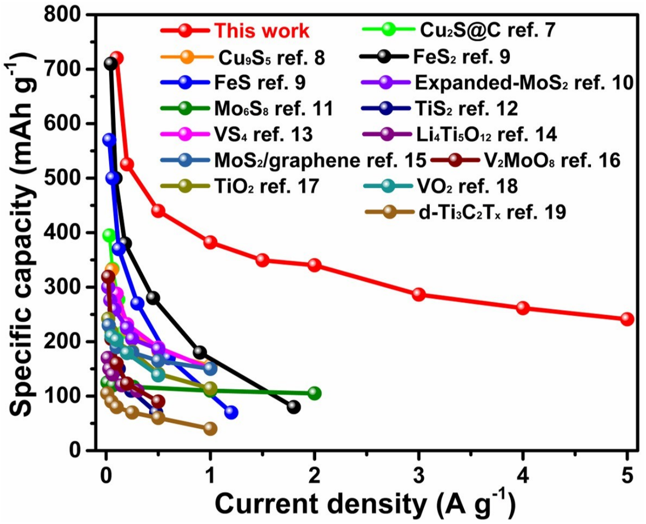

Fig. S11 Rate capability plot of MLIBs based on $TiO_{2-x}@CoS_2@PPy$ cathodes compared with other hybrid batteries reported in the literatures.

Table S1 Comparison of cycling performance of TiO_{2-x}@CoS_2@PPy with previous reported cathodes for MLIBs

Materials	Capacity	Retention	Reference
TiO_{2-x}@CoS_2@PPy	359.2 mAh g^{-1} after 2000 cycles at 1.0 A g^{-1}	~95.6%	This Work
	199.2 mAh g^{-1} after 5000 cycles at 5.0 A g^{-1}	~81.1%	
Cu_2S@C	150 mAh g^{-1} after 50 cycles at 0.03 A g^{-1}	~38.1%	Ref. 7
Cu_9S_5	156 mAh g^{-1} after 1000 cycles at 1.0 A g^{-1}	~84.0%	Ref. 8
FeS_2	210 mAh g^{-11} after 200 cycles at 0.09 A g^{-1}	~42.0%	Ref. 9
FeS	180 mAh g^{-1} after 150 cycles at 0.06 A g^{-1}	~32.7%	Ref. 9
Interlayer Expanded MoS_2	170 mAh g^{-1} after 500 cycles at 0.5 A g^{-1}	~75.2%	Ref. 10
Mo_6S_8	98 mAh g^{-1} after 3000 cycles at 1.3 A g^{-1}	~95.0%	Ref. 11
TiS_2	160 mAh g^{-1} after 400 cycles at 0.08 A g^{-1}	~99.0%	Ref. 12
VS_4	110 mAh g^{-1} after 1500 cycles at 1 A g^{-1}	~52.1%	Ref. 13
$Li_4Ti_5O_{12}$	120 mAh g^{-1} after 500 cycles at 0.06 A g^{-1}	~85.7%	Ref. 14
MoS_2/graphene	180 mAh g^{-1} after 200 cycles at 0.1 A g^{-1}	~90.0%	Ref. 15
V_2MoO_8	135.8 mAh g^{-1} after 50 cycles at 0.02 A g^{-1}	~72.5%	Ref. 16
VO_2	154.9 mAh g^{-1} after 100 cycles at 0.1 A g^{-1}	~75%	Ref. 18
d-$Ti_3C_2T_x$	73 mAh g^{-1} after 500 cycles at 0.1 A g^{-1}	~91.2%	Ref. 19

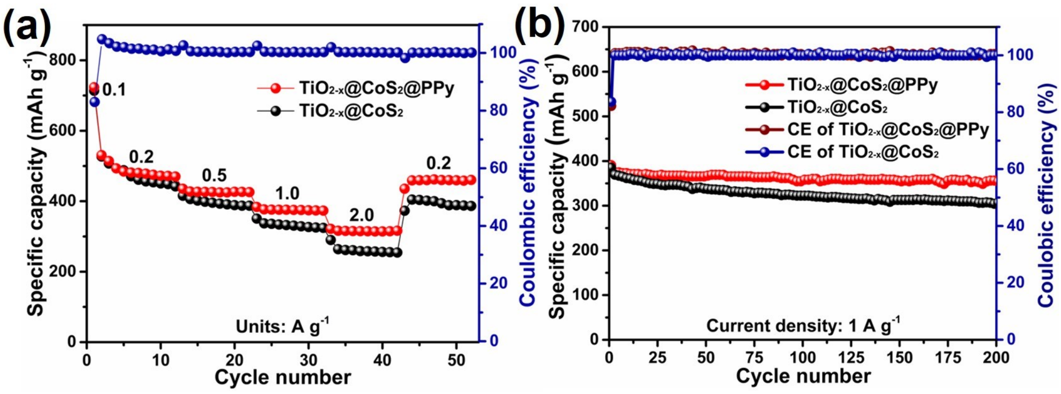

Fig. S12 (a) Rate capability and (b) cycling performances of the TiO$_{2-x}$@CoS$_2$@PPy and TiO$_{2-x}$@CoS$_2$ without PPy coating.

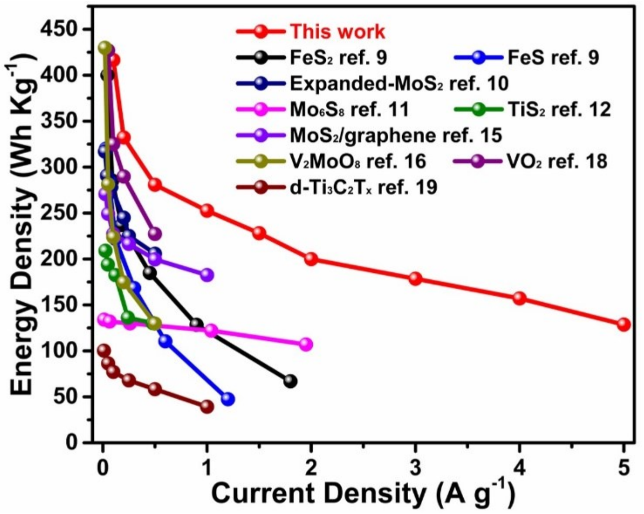

Fig. S13 Comparison of the energy density of TiO$_{2-x}$@CoS$_2$@PPy with previous materials in MLIB coin cell at different current densities.

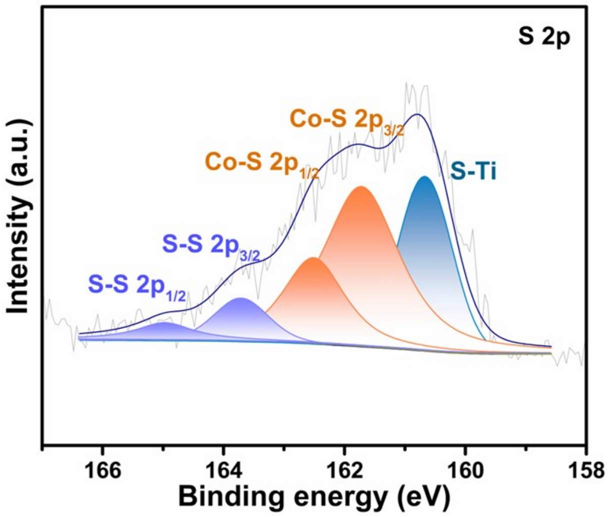

Fig. S14 High-resolution XPS spectra of S 2p in TiO_{2-x}@CoS_2@PPy after cycling test.

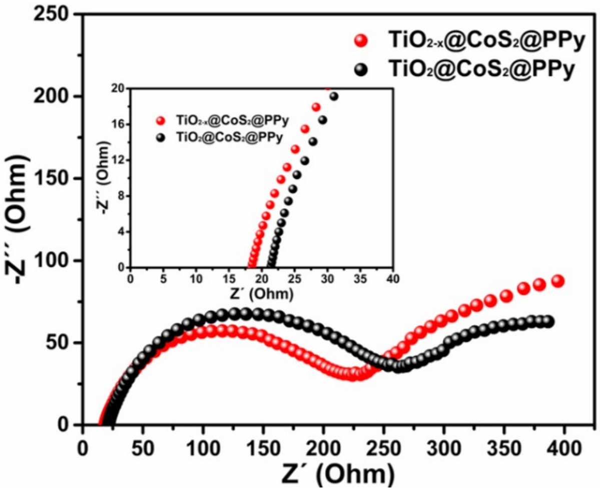

Fig. S15 EIS of TiO_{2-x}@CoS_2@PPy and TiO_2@CoS_2@PPy. Applied voltages are open circuit voltages; frequency range is from 10^6 to 10^{-1} Hz.

References

1. Q. An,; Y. Li, H. Deog Yoo, S. Chen, Q. Ru, L. Mai and Y. Yao, *Nano Energy*, **2015,** 18, 265-272.
2. J. P. Perdew, K. Burke and M. Ernzerhof, *Phys. Rev. Lett.*, **1996,** 77, 3865-3868.

3. P. E. Blochl, *Phys. Rev. B*, **1994,** 50, 17953-17979.
4. G. Kresse and J. Furthmüller, *Comp. Mater. Sci.*, **1996,** 6, 15-50.
5. G. Kresse and D. Joubert, *Phys. Rev. B*, **1999,** 59, 1758-1775.
6. S. Grimme, J. Antony, S. Ehrlich and H. Krieg, *J Chem Phys.*, **2010,** 132, 154104.
7. W. Wang, Y. Yang, Y. NuLi, J. Zhou, J. Yang and J. Wang, *J. Power Sources*, **2020**, 445, 227325.
8. T. Li, A. Qin, H. Wang, M. Wu, Y. Zhang, Y. Zhang, D. Zhang and F. Xu, *Electrochem. Acta*, **2018**, 263, 168-175.
9. Y. Zhang, J. Xie, Y. Han and C. Li, *Adv. Funct. Mater.*, **2015**, 25, 7300-7308.
10. X. Fan, R. R. Gaddam, N. A. Kumar and X. A Zhao, *Adv. Energy Mater.*, **2017**, 7, 1700317.
11. Y. Cheng, Y. Shao, J. Zhang, V. L. Sprenkle, J. Liu and G. Li, *Chem. Commun.*, **2014**, 50, 9644-9646.
12. T. Gao, F. Han, Y. Zhu, L. Suo, C. Luo, K. Xu and C. Wang, *Adv. Energy Mater.*, **2015**, 5, 1401507.
13. Y. Wang, C. Wang, X. Yi, Y. Hu, L. Wang, L. Ma, G. Zhu, T. Chen and Z. Jin, *Energy Storage Mater.*, **2019**, 23, 741-748.
14. N. Wu, Z. Yang, H. Yao, Y. Yin, L. Gu and Y. Guo, *Angew. Chem. Int. Ed.* **2015**, 54, 5757-5761.
15. C. Hsu, C. Chou, C. Yang, T. Lee and J. Chang, *Chem. Commun.*, **2016**, 52, 1701-1704.
16. X. Miao, Z. Chen, N. Wang, Y. Nuli, J. Wang, J. Yang and S. Hirano, *Nano energy*, **2017**, 34, 26-35.

17. Y. Meng, D. Wang, Y. Wei, K. Zhu, Y. Zhao, X. Bian, F. Du, B. Liu, Y. Gao and G. Chen, *J. Power Sources*, **2017**, 346, 134-142.

18. C. Pei, F. Xiong, J. Sheng, Y. Yin, S. Tan, D. Wang, C. Han, Q. An and L. Mai, *ACS Appl. Mater. Interfaces*, **2017**, 9, 17060-17066

19. A. Byeon, M. Zhao, C. Ren, J. Halim, S. Kota, P. Urbankowski, B. Anasori, M. Barsoum and Y. Gogotsi, *ACS Appl. Mater. Interfaces*, **2017**, 9, 4296-4300